

See discussions, stats, and author profiles for this publication at: <https://www.researchgate.net/publication/231648589>

In Situ Neutron Diffraction Study of the Deuteration of Isotopic (MgB₂)–B–11

ARTICLE *in* THE JOURNAL OF PHYSICAL CHEMISTRY C · OCTOBER 2011

Impact Factor: 4.77 · DOI: 10.1021/jp208355s

CITATIONS

12

READS

18

6 AUTHORS, INCLUDING:



[Jim Webb](#)

Griffith University

41 PUBLICATIONS 381 CITATIONS

[SEE PROFILE](#)



[Mark Paskevicius](#)

Aarhus University

54 PUBLICATIONS 679 CITATIONS

[SEE PROFILE](#)



[C.E. Buckley](#)

Curtin University

105 PUBLICATIONS 1,626 CITATIONS

[SEE PROFILE](#)



[Evan Gray](#)

Griffith University

30 PUBLICATIONS 404 CITATIONS

[SEE PROFILE](#)

In Situ Neutron Diffraction Study of the Deuteration of Isotopic Mg¹¹B₂

Mark P. Pitt,^{*,†,‡} Colin J. Webb,[†] Mark Paskevicius,[‡] Denis Sheptyakov,[§] Craig E. Buckley,[‡] and Evan MacA. Gray[†]

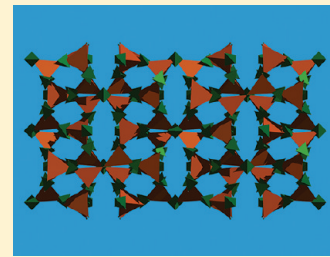
[†]Queensland Micro- and Nanotechnology Centre, Griffith University, Brisbane 4111, Australia

[‡]Department of Imaging and Applied Physics, Curtin University of Technology, GPO Box U 1987, Perth WA 6845, Australia

[§]Laboratory for Neutron Scattering, Paul Scherrer Institute, 5232 Villigen PSI, Switzerland

 Supporting Information

ABSTRACT: Isotopic Mg¹¹B₂ has been deuterated at 400 °C and 800 bar, with the production of β-Mg(¹¹BD₄)₂ observed by in situ neutron diffraction. A natural MgB₂ sample has been deuterated under similar conditions and studied ex situ by high resolution X-ray synchrotron diffraction. In both cases, quantitative phase analysis (QPA) indicates a ca. 43% yield of the high temperature (β) phase, with the rest of the sample composed of unreacted MgB₂ and Mg or MgD₂. A joint refinement of the neutron and X-ray synchrotron data has been performed, yielding a final β-Mg(¹¹BD₄)₂ structure in space group *Fddd*, with new D positions. Anisotropically broadened (odd, odd, odd) reflections are attributed to microstructural features, rather than antiphase boundaries. QPA of the isotopic sample indicates ca. 10% of B atoms are in a noncrystalline state. A broad feature is evident in the ex situ X-ray synchrotron data, covering a wide *d*-spacing range from ca. 3.80–5.45 Å, consistent with the formation of amorphous Mg(BD₄)₂ and amorphous B. For both samples, macroscopic fusing occurs, forming an extremely hard phase with a glassy black appearance, which is hydrogen impermeable and inhibits further formation of β-Mg(BH₄)₂. The fused surface regions of the sample have been studied by transmission (TEM) and scanning (SEM) electron microscopy. TEM studies show amorphous regions on the surface, consistent with amorphous B, and a Mg–B–O–H phase.



INTRODUCTION

In the quest to obtain reversible hydrogen storage materials of high gravimetric density and suitable thermodynamic properties, recent studies have concentrated on the group I and II metal borohydrides. Group I compounds such as LiBH₄ (18.5 wt % H) have proven to be too thermodynamically stable and are not reversible below their melting temperature; however, group II phases such as Mg(BH₄)₂ (14.9 wt % H) and Ca(BH₄)₂ (11.6 wt % H) are predicted to be less stable based on the variation of desorption temperature of M(BH₄)_n as a function of the electronegativity of M.¹ MgB₂ appears as a special case in the tetravalent complex hydride family (including alanates and borohydrides) where the stable intermetallic with the same atomic proportions of the hydride may be directly hydrogenated, in this case MgB₂ + 4H₂(g) → Mg(BH₄)₂. Other potential examples of direct hydrogenation of the intermetallic to form complex hydrides includes BeB₂ + 4H₂(g) → Be(BH₄)₂ and CaAl₂ + 4H₂(g) → Ca(AlH₄)₂. The solubility of hydrogen in MgB₂ has been of interest since the discovery of the enhancement of its high *T_c* (ca. 39 K)² superconducting properties induced by proton irradiation.^{3,4} At low hydrogen pressures, hydrogen atoms are absorbed into the MgB₂ lattice in weak concentrations to form a solid solution, which induces a resolvable ca. 0.6 K increase of *T_c*.⁵

The first stoichiometric hydride of MgB₂ was reported with the proportions Mg(BH₄)₂ over 60 years ago by wet chemical

synthesis;⁶ however, it has only very recently been structurally characterized.^{7,8} Both the low (α) and high (β) temperature Mg(BH₄)₂ phases reported possess remarkable structural complexity. There have been numerous ground state Mg(BH₄)₂ structures predicted by density functional theory (DFT),^{9–13} none of which matched the experimentally determined structures. Both the α -Mg(BH₄)₂ and β -Mg(BH₄)₂ structures are reported from X-ray synchrotron data, in hexagonal space group *P6*₁ (*a* = 10.341 Å, *c* = 37.086 Å) and orthorhombic *Fddd* (*a* = 37.072 Å, *b* = 18.648 Å, *c* = 10.912 Å), respectively.⁷ The α -Mg(BD₄)₂ structure was also solved by joint refinement of X-ray synchrotron and neutron data, using natural B.⁸ The space group of the α -Mg(BH₄)₂ phase was recently revised as *P6*₁22 using single crystals,¹⁴ with longer B–H and H–H separation, according to a DFT relaxation of the *P6*₁ structure.¹⁵ It is also noted from relaxation of the *P6*₁ structure that all B–H distances fall in the range 1.22–1.23 Å, indicating that all BH₄[−] tetrahedra are near identical.¹⁶ The α and β structure types are atypical, with Mg²⁺ cations coordinated tetrahedrally by BH₄[−] units, resulting in a unique eightfold coordination of Mg by H.^{8,14} The distorted Mg²⁺[BH₄[−]]₄ tetrahedra form a corner sharing 3D network,

Received: August 30, 2011

Revised: October 5, 2011

Published: October 06, 2011

with each $[\text{BH}_4^-]$ unit approximately linearly coordinated by two Mg^{2+} ions. These 3D networks also include large open pores. It is noted that the complexity of these structures is dependent on ionic charge transfer.¹⁷ Other structural forms of $\text{Mg}(\text{BH}_4)_2$ have also been identified. $\gamma\text{-Mg}(\text{BH}_4)_2$ (unindexed) was obtained by ball milling $\beta\text{-Mg}(\text{BH}_4)_2$ with SiO_2 or Al_2O_3 ,¹⁸ another hexagonal phase (different from the α form) was indexed in space group $P6_3$ ($a = 8.35 \text{ \AA}$, $c = 4.68 \text{ \AA}$), obtained at pressures $>3.35 \text{ GPa}$,¹⁹ and in the earliest decomposition studies, a tetragonal ($a = 13.59 \text{ \AA}$, $c = 16.51 \text{ \AA}$) and a face-centered cubic form ($a = 15.5 \text{ \AA}$) were identified.²⁰ It is highly likely that many structural variations of $\text{Mg}(\text{BH}_4)_2$ exist, which may be sensitive to synthesis conditions and/or oxide-based impurities. Many of these structures may be near degenerate in energy, which could explain the difficulty in correctly modeling and predicting these structure types by DFT. It has also been noted that porous $\text{Mg}(\text{BH}_4)_2$ structures are analogous to zeolitic materials including silica,¹⁵ which is known to possess a wide variety of structures with similar energy, and where the preparation conditions determine the final structure.²¹

Two recent studies exist describing the direct hydrogenation of MgB_2 . In the first study, MgB_2 was hydrided at 950 bar and 400°C for 108 h to yield ca. 75% $\beta\text{-Mg}(\text{BH}_4)_2$.²² Attempts to lower the hydrogenation temperature with numerous transition-metal additives were unsuccessful. In the second study, $\text{Mg}(\text{BH}_4)_2$ decomposed up to 600°C (with and without additives) was rehydrided at 900 bar and 390°C for 78 h.²³ Ca. 66% conversion to $\beta\text{-Mg}(\text{BH}_4)_2$ was achieved for the pure sample, with a significant quantity of unreacted MgB_2 evident in the diffraction data. While the TiF_3 and ScCl_3 additives significantly improved the desorption of hydrogen from $\text{Mg}(\text{BH}_4)_2$ at 300°C , their presence during reabsorption was reported to increase the proportion of $\text{Mg}(\text{B}_x\text{H}_y)_n$ type phases. Previous studies of H sorption in MgB_2 also exist from attempts to modify the superconducting properties of MgB_2 . During the synthesis of MgB_2 in a 10 bar hydrogen atmosphere, temperatures $>1000 \text{ K}$ were required to obtain a high yield of MgB_2H_x (ca. 0.01 mass % H total) over a period of hours.⁵ A high pressure study has shown that an applied pressure of 20–7000 bar at 100°C made no difference to the amount of hydrogen absorbed by MgB_2 , to a final composition of $\text{MgB}_2\text{H}_{0.03}$.²⁴ The same study also shows that MgB_2 decomposes (presumably to $\text{Mg} + 2\text{B}$) at 250°C and 0.5–20 bar $\text{H}_2(\text{g})$ pressure. The above results indicate that the hydrogenation of MgB_2 is significantly kinetically stable (highly likely due to the construction of immense superstructures requiring long-ranged transport of both metal and H species at temperatures $\gg 100^\circ\text{C}$); thus, long hydrogenation times are necessary. The use of transition metal additives appears unnecessary, and unbeneficial in terms of producing stable $\text{Mg}(\text{B}_x\text{H}_y)_n$ type phases which hinder further reaction. This is also consistent with DFT studies,²⁵ which suggest that MgB_2 surfaces are highly favorable for H_2 dissociation and barrier-less local H transport, indicating that MgB_2 by itself performs the function of a catalytic additive.

Studies of the decomposition mechanism of $\text{Mg}(\text{BH}_4)_2$ have been conducted since the earliest report in 1952,²⁶ proposing the reaction $\text{Mg}(\text{BH}_4)_2 \rightarrow \text{Mg} + 2\text{BH} + 3\text{H}_2(\text{g})$. The first thermal data showed a polymorphic transformation at 180°C ,²⁷ the first description of what is now understood as the α ($P6_{12}2$) to β ($Fddd$) transformation, which apparently leaves antiphase domains in the $\beta\text{-Mg}(\text{BH}_4)_2$ structure type, unique among the known Group I and II polymorphic transformations.^{28,29} Beyond the polymorphic transition, several endothermic events can generally be observed up to 500°C ,^{30–34} accompanied by the

release of H, which are known to be back-pressure dependent.³² The multiplicity of endothermic events in differential scanning calorimetry (DSC) data suggests a multistep dehydrating mechanism for $\text{Mg}(\text{BH}_4)_2$, accompanied by the formation of intermediate phases. Thermodynamically, the overall decomposition reaction is estimated experimentally to be ca. 67 kJ/mol $\text{Mg}(\text{BH}_4)_2$ ³¹ and ca. 57 kJ/mol H_2 from pressure–composition–temperature (PCT) data.³² Interpretation of the multistep decomposition mechanism is problematic due to the lack of crystalline phases appearing in diffraction data and very broad features appearing at high d -spacings (4.75–4.89 \AA interpolated from published X-ray diffraction data, with no knowledge of the zero offset),^{30,32,33,35,36} suggesting either amorphous or highly nanocrystalline phases. Based on ex situ diffraction studies, a similar five-step mechanism (linked with endothermic events) can be observed.^{32,33} Step I involves the release of H up to the melting point (T_m) of $\text{Mg}(\text{BH}_4)_2$, ca. 290°C , after which the diffraction pattern appears featureless, and no crystalline reflections are evident. Step II involves the release of the largest quantity of H from the sample, until the formation of MgH_2 is observed at ca. 330 – 360°C . Step III is the release of H from MgH_2 , typically up to $>400^\circ\text{C}$, with step IV showing the formation of elemental Mg, and step V showing the formation of MgB_2 at very high temperature, up to 580°C (dependent on sample oxidation). It is noted that no B containing crystalline phases are observed until MgB_2 growth after 410°C .³² A very similar mechanism was observed by in situ X-ray diffraction,³⁷ with a featureless diffraction pattern extending from ca. 300 – 350°C before MgH_2 formation.

Due to the featureless diffraction data obtained over a temperature range including at least two endothermic events, spectroscopic techniques have been applied, including nuclear magnetic resonance (NMR) and Raman spectroscopy. After $\text{Mg}(\text{BH}_4)_2$ desorption up to 300°C , Raman spectra show features which are not attributable to either $\text{Mg}(\text{BH}_4)_2$ (in either the crystalline or ball-milled state) or the decomposed products (MgB_2), suggesting that at temperatures $>300^\circ\text{C}$, new and unidentified intermediate phases have appeared.²³ Solid state ^{11}B NMR spectra shows a chemical shift starting at ca. -20 ppm , which shifts to -12 ppm after heating above 400°C .^{37,38} The -12 ppm peak apparently cannot be assigned to amorphous boron or any $\text{Mg}(\text{BH}_4)_2$ phase. The existence of ^1H – ^{11}B coupling indicates the presence of a B_nH_m species³⁷ with B–H bond length of ca. 1.2 \AA (22 kHz).³⁸ Further comparison to a crystalline $\text{K}_2\text{B}_{12}\text{H}_{12}$ spectrum shows matching of the -12 ppm peak, suggesting the possibility of a polyhedral $\text{MgB}_{12}\text{H}_{12}$ species forming as an intermediate. A multistep decomposition based on $\text{MgB}_{12}\text{H}_{12}$ formation was thus proposed.^{37,38} Further solid state and solution ^{11}B NMR were carried out, where $\text{Mg}(\text{BH}_4)_2$ was slowly desorbed at 200°C over a 5 week period with the proposed formation of a metastable triborane species $\text{Mg}(\text{B}_3\text{H}_8)_2$.³⁹ A more complex decomposition pathway involving B_2H_6 and MgB_2H_7 was proposed. An even more complex seven-step pathway involving MgB_2H_6 , MgB_2H_7 , “ MgBH_4 ”, $\text{MgB}_{12}\text{H}_{12}$ and MgB_4 formation has been proposed based on pressure–composition isotherms and DSC.²¹ While numerous experimental^{21,22,33,35,37,38} and DFT^{9,11,40,41} studies have proposed the formation of a stable intermediate $\text{MgB}_{12}\text{H}_{12}$ species, it should be noted that the single phase anhydrous crystalline form of $\text{MgB}_{12}\text{H}_{12}$ has currently not been synthesized,⁴² which is surprising considering its proposed high stability.

Taken together, the experimental findings and modeling analysis to date suggest that while the MgB₂ surface may be favorable in hydrogenation terms and has no need for catalytic additives, the transport of H through the MgB₂ bulk is likely kinetically hindered. Therefore this system requires (a) high temperature to drive both H and metal transport to build the β -Mg(BH₄)₂ superstructure and (b) high hydrogen pressure to avoid decomposition into Mg + 2B (or potentially Mg_xB_yH_z) at 250 °C²⁴ under low hydrogen pressures. The kinetic stability in this system that hinders H motion/transport is consistent with the irreversible transformation from the high temperature Mg(BH₄)₂ structure to the low temperature Mg(BH₄)₂ structure at ca. 190 °C.⁷ In addition, the formation of stable intermediate Mg_xB_yH_z containing phases during the hydrogen cycling of metal borohydrides is highly detrimental to their practical application.

In this study, we follow the formation of the isotopic β -Mg(¹¹BD₄)₂ superstructure at 400 °C and 800 bar by in situ neutron diffraction. We revise the *Fddd* structure proposed for high temperature Mg(BH₄)₂ phase⁷ and study the surface regions of fused samples by high resolution TEM to understand what phases have formed and why they are impermeable to hydrogen.

■ EXPERIMENTAL DETAILS

MgB₂ (natural B) –325 mesh >96% purity and Mg chips of 99.98% purity were purchased from Sigma-Aldrich. Isotopic ¹¹B (99%) was purchased from Cambridge Isotope Laboratories, Inc. All powder handling was performed in an Ar glovebox, with O₂ and H₂O < 1 ppm. Isotopic Mg¹¹B₂ was prepared by heating Mg:¹¹B in a 1:2 molar proportion in a Mo boat, up to 850 °C under 50 bar of high purity Ar for 2 h in a sealed furnace, according to literature.⁴³ Mg¹¹B₂ yield was 89.4 mol %, with the remainder of the sample consisting of unreacted Mg (8.4 mol %) and MgO (2.2 mol %). This isotopic Mg¹¹B₂ sample was used without further modification for in situ neutron diffraction measurements. Natural MgB₂ was commilled with 5 mol % Al₃Ti (as a catalytic additive) in a hardened and tempered Inconel vial. Milling was performed with a 1 g sample, 5 Inconel balls (10 mm diameter), a 20:1 ball to powder ratio, at 600 rpm, under Ar, in a Fritsch P6 mill, for 30 min. The Al₃Ti additive was prepared from an Al₃Ti arc melt (flipped 10 times) using Al lumps (10 mm 99.999%) from Goodfellow and Ti granules (–15 mesh 99.95%) from Sigma Aldrich. The Al₃Ti arc melt was crushed and milled under 85 bar H₂ for 100 h in a hardened and tempered tool steel vial/balls to break down the particle size, with similar milling parameters described above. The natural MgB₂ + 0.05Al₃Ti sample was deuterated under 1650 bar at 350 °C for ca. 12 h, using a high pressure Sieverts apparatus composed of commercial Sno-Trik valves and fittings rated to 3000 bar and a custom Inconel cell rated to 600 °C and 5000 bar. After cooling to room temperature, the natural MgB₂ + 0.05Al₃Ti sample was removed, ground, and loaded in a 0.8 mm quartz capillary for ex situ X-ray synchrotron measurements. The isotopic Mg¹¹B₂ sample was loaded in a custom neutron cell, manufactured from hot isostatically pressed Ti_{2.08}Zr. The cell has an internal thin-walled AISI316 liner to protect the Ti_{2.08}Zr cell body from hydrogen embrittlement⁴⁴ and is rated to 1000 bar at 400 °C. The neutron cell forms part of an in situ Sieverts apparatus, constructed from commercial 1000 bar SITEC valves and fittings. The isotopic Mg¹¹B₂ sample was deuterated up to 400 °C under 800 bar deuterium pressure. Ex situ high resolution X-ray synchrotron diffraction data were collected on the Powder Diffraction Beamline at the Australian

Table 1. Deuteration/Hydrogenation Conditions and Experimental Technique Applied To Obtain Magnesium Borohydride Samples

	sample 1	sample 2	sample 3
composition	Mg ¹¹ B ₂ + D ₂ (g)	MgB ₂ + 0.05Al ₃ Ti + D ₂ (g)	MgB ₂ + H ₂ (g)
experiment	in situ neutron diffraction	ex situ X-ray synchrotron diffraction	TEM/SEM
pressure (bar)	800	1650	800
temperature (°C)	400	350	400
time (h)	34	12	24

Synchrotron in Melbourne, Australia. High resolution data ($\Delta d/d \sim 3 \times 10^{-4}$) were collected at 295 K between 2 and 81° 2θ, binned in steps of 0.004°. A wavelength of 0.8272 Å was obtained from a flat crystal pair Si(111) monochromator. The instrumental X-ray diffraction profile was characterized by a NIST 660a LaB₆ line shape standard. In situ neutron diffraction data were collected using the High-Resolution Powder Diffractometer for Thermal Neutrons (HRPT) at the Laboratory for Neutron Scattering, Paul Scherrer Institute, Switzerland. Medium resolution data ($\Delta d/d \sim 1 \times 10^{-3}$) were collected up to 400 °C and 800 bar between 4 and 165° 2θ, binned in steps of 0.05°. A wavelength of 1.4942 Å was obtained from a vertically focusing Ge (533) monochromator. The instrumental neutron diffraction profile was characterized by a Na₂Ca₃Al₂F₁₄ fluorite standard. X-ray synchrotron and neutron diffraction patterns were analyzed by the Rietveld method using RIETICA⁴⁵ and Topas (Bruker AXS). Diffraction line shape profiles were fitted with a full Voigt or pseudo-Voigt function. The β -Mg(¹¹BD₄)₂ structure was modeled in space group *Fddd*. A third natural MgB₂ sample was hydrided under similar conditions to the isotopic Mg¹¹B₂ sample, and after cooling to room temperature, the sample was measured in the absorbed state by high resolution TEM. Synthesis conditions for all samples are detailed in Table 1. Measurements were conducted on a JEOL 3000F FEGTEM instrument operating at 300 kV. The TEM was equipped with an Oxford Instruments EDS detector for elemental analysis. Samples were loaded onto 200 mesh copper grids with holey carbon support films dropwise via suspension in toluene. Sample loading into the TEM column was undertaken within an argon filled glovebag to reduce oxidation due to air exposure. Scanning electron microscopy (SEM) was conducted on a Zeiss Evo 40XVP instrument operating up to 30 keV with both secondary electron (SE) and backscattered electron (BSE) detectors. The SEM was equipped with an Oxford Instruments EDS detector for elemental analysis. Samples were gold coated to prevent charging and were briefly exposed to air upon loading into the SEM column (less than 1 min). The infrared spectrum was collected using a Bruker IFS 66 FT-IR with 64 background and 64 sample scans, coaveraged and ratioed. A water-cooled globar source and a room-temperature deuterated triglycine sulfate (DTGS) detector were used. The spectrometer was purged with dry nitrogen. Samples were prepared by encapsulation within pressed KBr pellets.

■ RESULTS AND DISCUSSION

Joint Refinement of X-ray Synchrotron and Neutron Data. In the combination plot in Figure 1, we show the diffraction data

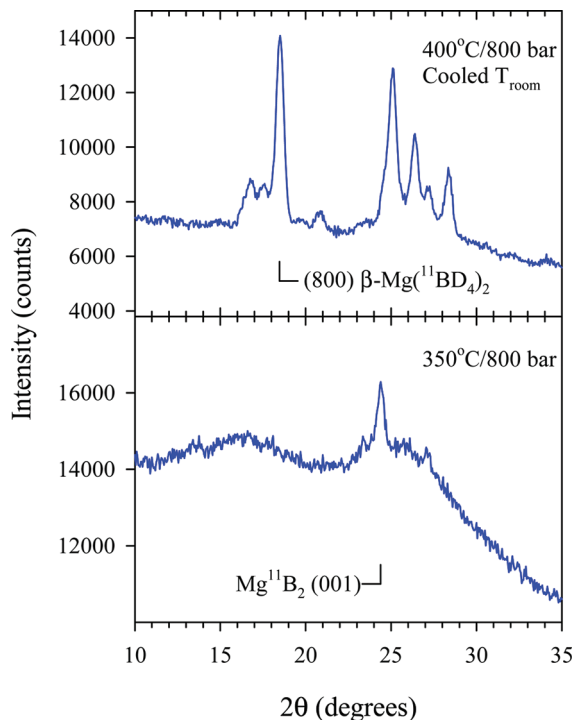


Figure 1. Neutron diffraction data showing two distinctly broad peaks at 350 °C/800 bar before commencing cooling (bottom) and crystallization of the high temperature β -Mg($^{11}\text{BD}_4$)₂ phase after cooling from 400 °C and 800 bar to room temperature (top).

from isotopic Mg $^{11}\text{B}_2$ after 28 h at 350 °C and 800 bar D₂ pressure (lower figure), during which time our manometry indicated significant deuterium absorption by the sample, ca. 11.84 wt % D. No significant absorption of deuterium occurred at temperatures below 350 °C. Very broad features can be observed at ca. 16.23 and 25.84° 2θ, immediately in the vicinity where strong crystalline reflections of the β -Mg($^{11}\text{BD}_4$)₂ appear after the sample is cooled to room temperature (upper figure). At 400 °C and 800 bar, the neutron diffraction pattern remained similar to that in the lower figure, with a further 5.07 wt % D absorbed, giving a total of 16.91 wt % D absorbed by the sample. The very broad features suggest that nanocrystals of β -Mg($^{11}\text{BD}_4$)₂ have formed at 350 °C and 800 bar, beyond the melting temperature of the β -phase at ca. 290 °C. Cooling the sample to room temperature has crystallized a large amount of the β -Mg($^{11}\text{BD}_4$)₂ phase, on average a ca. 43% yield. Quantitative phase analysis (QPA) indicates ca. 10% of B atoms are in a noncrystalline state (see the following section), consistent with macroscopic sample fusing occurring (see the final section for a concise description of this process).

We initially attempted to fit the β -Mg(BH_4)₂ structure⁷ to our neutron data, by simply replacing B with ^{11}B and H with D. The difference profile in Figure 2 shows that the fit quality is suffering from significant intensity misfits, particularly in the 30–40° 2θ region, where the calculated model is producing intensity when there is very little intensity in the data. As discussed in ref 7, the H positions have been fixed in ideal BH_4^- tetrahedra, and there are too many parameters to uniquely locate the H atoms with only X-ray data. Aside from the issue of locating H atoms with X-ray data, there also exist problems with interatomic distances in the proposed structure determination.⁷ B–H = 1.01–1.02 Å, H–H = 1.66 Å, Mg–H = 1.70–1.75 Å, and Mg–B = 2.32–2.49 Å are all

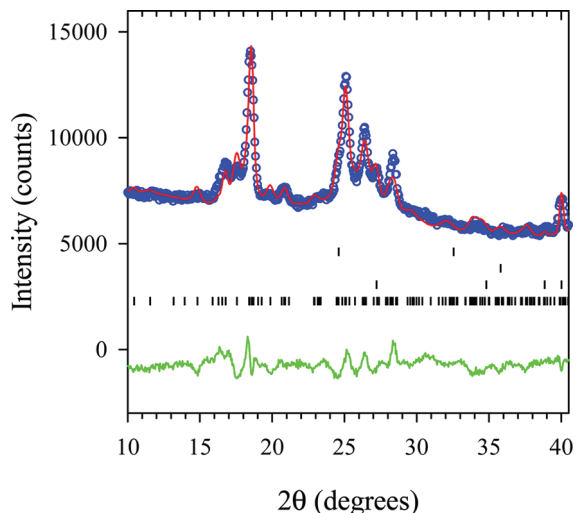


Figure 2. Fit of the proposed *Fddd* β -Mg(BH_4)₂ structure⁷ to our neutron data, replacing B with ^{11}B and H with D. Significant intensity misfit is evident, indicating the structure needs revision. Reflection markers from top to bottom represent Mg $^{11}\text{B}_2$, MgO, MgD₂, and β -Mg($^{11}\text{BD}_4$)₂.

very short and unphysical bond lengths, and from this perspective, the proposed structure solution of β -Mg(BH_4)₂ phase⁷ must be considered a false minimum with regard to the H positions.

Our first approach in revising the proposed β -Mg(BH_4)₂ structure⁷ was to refit our neutron data, with antibump separations of B–D = 1.23 Å, D–D = 2.10 Å, Mg–D = 1.95 Å, and Mg– ^{11}B = 2.50 Å. Constraining the $^{11}\text{BD}_4^-$ tetrahedra and allowing all atomic positions to relax allowed us to obtain an excellent fit to the neutron data. However, this structure solution was a poor quality fit to our X-ray synchrotron data. It was clear that fitting either the neutron data or X-ray synchrotron data by themselves yielded false minima, and a joint refinement was necessary to obtain the correct structure solution. To model the broad (odd, odd, odd) reflections that are more easily observed in the higher resolution X-ray synchrotron data, we have used a simple broadening model, rather than an antiphase model. While antiphase domains are plausible, the broadening could also equally likely be from a microstructural defect, such as free edge or screw dislocations. Either of these possibilities could in principle be directly tested by TEM, but in practice complex hydrides suffer considerable high energy “knock on” electron beam damage, associated with the rapid evaporation of hydrogen and even light metals from the sample,⁴⁶ destroying the original features in the sample. Figure 3 shows the final excellent fit quality from the joint refinement of the average β -phase structure against the neutron and X-ray synchrotron data. While the X-ray synchrotron measurements in ref 7 have provided good knowledge of the atomic coordinates of the Mg/B substructure, all H atoms have moved to fit the neutron data, which will change the final calculated energy of the structure. The change in the eightfold H coordination environment around Mg from the proposed structure⁷ to our new joint refined structure is shown in Figure 4. Our Mg and B positions are in good agreement with the Mg/B positions in the proposed structure⁷ (only a minor shift of the Mg/B substructure occurs in the joint refinement); however, it is clear that all BD_4^- tetrahedra are rotated, yielding new D positions. Longer edges can also be discerned on our BD_4^- tetrahedra. To preserve the MgH₈ coordination environment, opposing edges of BH_4^-

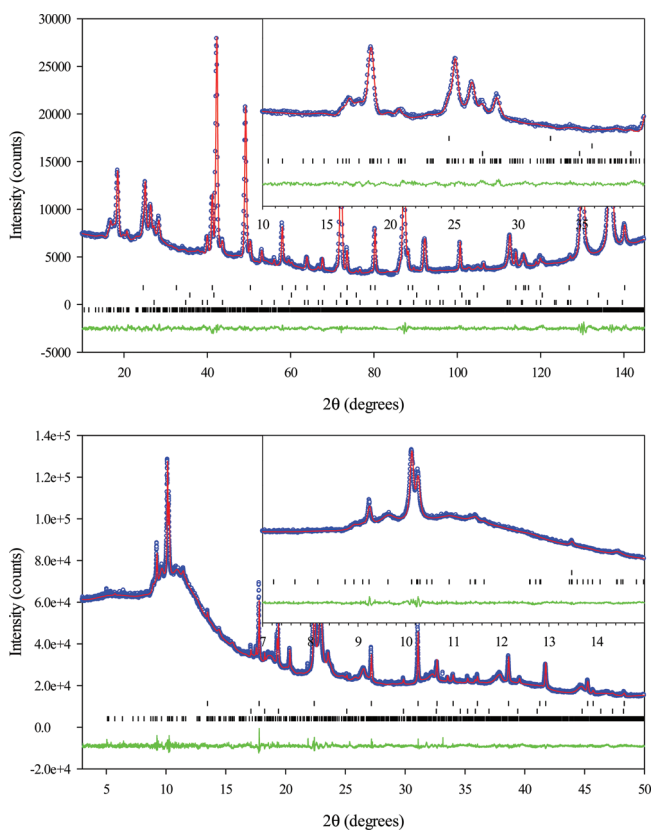


Figure 3. Joint refinement of neutron data from deuterated isotopic $^{11}\text{MgB}_2$ (upper figure) and X-ray synchrotron data from deuterated natural $\text{MgB}_2 + 0.05\text{Al}_3\text{Ti}$ (lower figure). Reflection markers from top to bottom represent (i) Mg^{11}B_2 , MgO , MgD_2 and $\beta\text{-Mg}^{(11)}\text{BD}_4)_2$ (neutron data) and (ii) MgB_2 , Mg , and $\beta\text{-Mg}(\text{BD}_4)_2$ (X-ray synchrotron data). Experimental data points are represented by open circles, and the solid line represents the Rietveld calculation, with the difference profile given below the reflection markers. Insets show the fit quality in regions corresponding to the strongest intensities of the high temperature β -phase.

tetrahedra need to be aligned toward Mg^{2+} cations, and in some BH_4^- tetrahedra from the proposed structure solution in ref 7 the MgH_8 symmetry is broken, and a tetrahedral face is tilted toward Mg resulting in two long and one short Mg–H distance, instead of two short and one long. This results in a wider spread of Mg–H distances from the proposed structure solution in ref 7 compared to our solution, as shown in the comparison of Mg–H bond length distributions shown in the inset figures in Figure 4. The final structural details of our $\beta\text{-Mg}^{(11)}\text{BD}_4)_2$ structure solution are reported in the Supporting Information. The average structure remains symmetrically similar to the originally proposed structure solution,⁷ with distorted $\text{Mg}^{2+}[\text{BD}_4^-]_4$ tetrahedra forming a corner sharing 3D network, with each corner sharing $[\text{BD}_4^-]$ unit approximately linearly coordinated by two Mg^{2+} ions, with $\text{Mg}^{2+} \cdots \text{BD}_4^- \cdots \text{Mg}^{2+}$ angles in the range $140.62\text{--}159.16^\circ$. Table 2 presents a comparison of interatomic separations from all experimentally determined α and β phase structures, and the recently determined γ and δ phase structures,⁴⁷ together with 0 K bond lengths from ground state structures predicted by density functional theory (DFT).¹⁵

QPA of the X-ray Synchrotron and Neutron Data. In both cases, deuteration of our natural MgB_2 and isotopic Mg^{11}B_2 samples resulted in a ca. 43% yield of the high temperature

$\beta\text{-Mg}(\text{BD}_4)_2$ phase. The difference in maximum sample pressure of 1650 bar on the natural MgB_2 compared to 800 bar on the isotopic Mg^{11}B_2 has apparently resulted in different proportions in the remaining phases in the samples. The isotopic sample clearly contains more “free” Mg that has deuterated to MgD_2 (as there exists significant free Mg in the as prepared isotopic Mg^{11}B_2), but in the case of the natural sample, the free Mg remains unreacted and does not contain deuterium, even though the sample has been under an additional 850 bar of pressure. QPA of the deuterated natural MgB_2 sample indicates ca. 4.3% of B atoms are in a noncrystalline state, while in the deuterated isotopic Mg^{11}B_2 sample, the “missing” B is ca. 10%. In both samples, all of the Mg is accounted for in crystalline phases, and only B appears to be in a noncrystalline state. The major difference between the natural and isotopic samples is the maximum pressure applied. The higher maximum pressure of ca. 1650 bar on the natural sample appears to have hindered/decreased the formation of free Mg. Due to the presence of Mg (and not MgD_2) in the natural sample, it appears that this Mg is inaccessible to deuterium, suggesting a morphology where the free Mg is trapped behind a deuterium impermeable layer. Such an impermeable layer must also exist for the isotopic sample, as in both cases, almost one-third of the sample remains as unreacted microcrystalline MgB_2 . However, the location of free Mg in the isotopic sample appears to be morphologically different and accessible to deuterium, suggesting it is in front, or embedded on the surface of the deuterium impermeable layer. The formation of this deuterium impermeable layer is consistent with the 4–10% missing or noncrystalline B. As the QPA indicates only B is in a noncrystalline state, this suggests the deuterium impermeable layer is composed of amorphous or highly nanocrystalline B.

The primary halo from amorphous B is typically observed at ca. 4.4 \AA .^{48,49} Inspection of our ex situ X-ray synchrotron data in Figure 5 shows a very broad feature covering a wide d -spacing range from ca. $3.80\text{--}5.45\text{ \AA}$, which includes potential primary halos with maxima at $d = 4.75\text{--}4.89\text{ \AA}$ for amorphous $\text{Mg}(\text{BH}_4)_2$,^{30,32,33,35,36} amorphous B at $d = 4.40\text{ \AA}$, and the halo from the quartz capillary, typically observed at ca. $d = 4.00\text{--}4.10\text{ \AA}$. There may also be residual nanocrystals of $\beta\text{-Mg}(\text{BH}_4)_2$ contributing to the intensity in this region. Inspection of the quartz halo from the pure MgB_2 sample indicates it contributes less than half of the total intensity in the $3.80\text{--}5.45\text{ \AA}$ region. The quartz halo in Figure 5 has been modeled (width and intensity) directly from the pure MgB_2 sample. The B halo has been modeled at the same width as literature data.⁴⁹ The primary halos shown in Figure 5 have not been fitted and are only presented as an aid to the eye to discriminate the proportion of the intensity covering the $3.80\text{--}5.45\text{ \AA}$ region to which they contribute. Amorphous $\text{Mg}(\text{BH}_4)_2$ crystallizes at a relatively low temperature, ca. 108°C , accompanied by a small exothermic spike in DSC data.³⁰ Based on the exothermic DSC spike, amorphous $\text{Mg}(\text{BH}_4)_2$ cannot take part in the hydrogen absorption process at high temperatures $\gg 100^\circ\text{C}$, and this is also the case for the decomposition process, where the diffraction patterns begin to appear featureless after ca. 300°C . However, it should be noted from in situ data that crystallization of amorphous $\text{Mg}(\text{BH}_4)_2$ continues up to ca. 250°C ,³⁶ evidenced by the halo beginning to lose intensity after ca. 185°C , commensurate with the polymorphic transition, indicating that amorphous $\text{Mg}(\text{BH}_4)_2$ crystallizes over a wide temperature range and may simultaneously crystallize both the α and β phase. The amorphous $\text{Mg}(\text{BH}_4)_2$ halo has disappeared before reaching 300°C . The appearance of the amorphous $\text{Mg}(\text{BH}_4)_2$ halo in many ex situ X-ray diffraction patterns

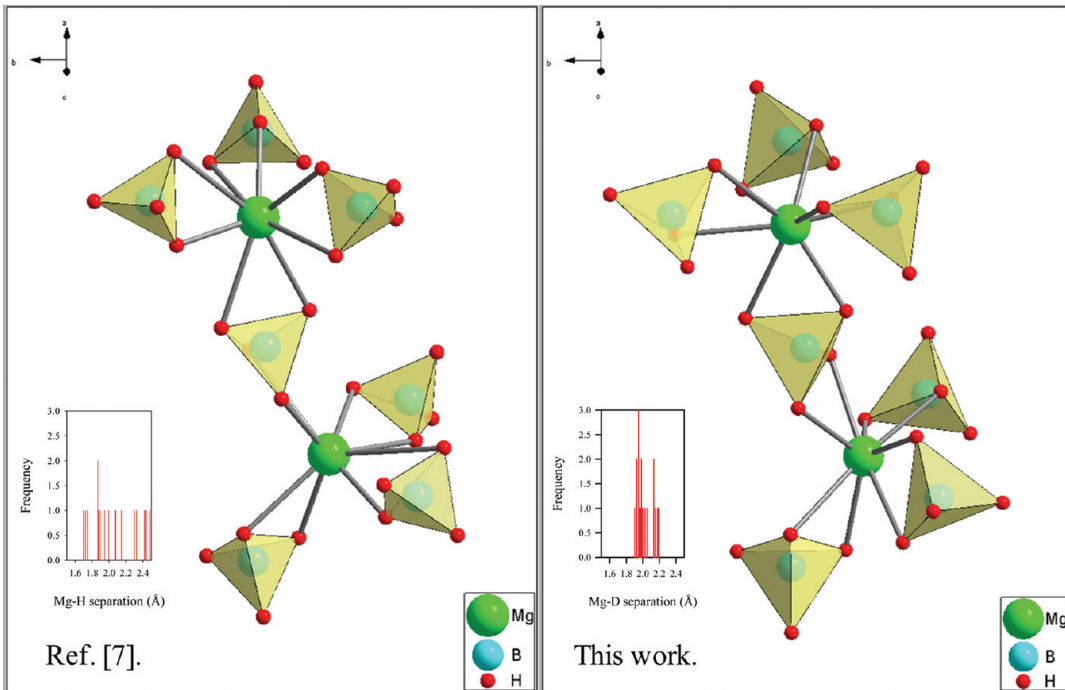


Figure 4. Changes in the eightfold hydrogen coordination environment of Mg cations, from the originally proposed structure solution⁷ (left), compared to our jointly refined structure (right). BD₄⁻ tetrahedra are rotated compared to the original structure,⁷ with new D positions.

Table 2. Comparison of Interatomic Distances (in Å) from All Experimentally Determined and 0 K DFT Ground State Crystal Structures for α , β , δ , and γ -Mg(BH₄)₂^a

	α -Mg(BH ₄) ₂ ref 7	β -Mg(BH ₄) ₂ ref 7	α -Mg(BH ₄) ₂ ref 14	β -Mg(BH ₄) ₂ ref 15 DFT	γ -Mg(BH ₄) ₂ ref 47	δ -Mg(BH ₄) ₂ ref 47	β -Mg(¹¹ BD ₄) ₂ this work.
Mg–B	2.282–2.571	2.340–2.492	2.391–2.448	2.361–2.432	2.413	2.438–2.486	2.333–2.452
Mg–H (MgH ₈)	1.759–2.368	1.698–2.441	1.907–2.192	1.994–2.183	1.958–1.998	1.962–2.139	1.904–2.190
B–H	1.120–1.128	1.013–1.020	1.114–1.119	1.218–1.231	1.220	1.213–1.216	1.230
H–H (in)	1.835	1.659	1.708–1.890	1.941–2.074	1.991–1.992	1.980–1.992	1.995–2.016
H–H (out)	> 2.213	> 1.985	> 2.315	> 2.187	> 2.274	> 1.725	> 2.096

^a H–H (in) refers to H–H bonding within BH₄ tetrahedra, H–H (out) to minimum H–H separation between BH₄ tetrahedra.

from >300 °C^{32,33,35} is evidently an artifact of sample cooling conditions.

Manometric measurements show that the absorption of deuterium by the isotopic Mg¹¹B₂ sample has stopped at 400 °C, which indicates the deuterium impermeable phase has formed in sufficient quantity at high temperature to hinder further deuterium absorption. Although isotropic incoherent scattering and an order of magnitude reduction in scattering power render the identification of amorphous features more difficult in neutron diffraction data, there are distinctly observable background deviations which run across the maximum for amorphous B at $d = 4.40$ Å. Figure 6 shows that at 350 °C and 800 bar (lower figure), the broad features from apparently nanocrystalline β -Mg(¹¹BD₄)₂ dominate, and it is difficult to discern the contribution of the primary amorphous halo from B. After the sample has cooled from 400 °C and 800 bar (upper figure), some deviation remains; however, it could be attributed to the incomplete crystallization of β -Mg(¹¹BD₄)₂, and nanocrystals may remain in the sample. Clearly it is preferable to use X-ray synchrotron data from samples contained in crystalline capillaries to observe amorphous halos.

Figure 7 shows the neutron diffraction cooling sequence (left figure) from ca. 400 to 145 °C. Upon close inspection, it is clear that the diffraction pattern displays only the two broad features at 16.23 and 25.84° 2θ, until the onset of the polymorphic transition temperature, where at ca. 184 °C, strong crystalline reflections from the β -Mg(¹¹BD₄)₂ phase appear. Slightly above 184 °C, the reflections of the crystalline β -Mg(¹¹BD₄)₂ phase are becoming discernible close to the very broad features at ca. 16.23 and 25.84° 2θ, and QPA (right figure in Figure 7) indicates that ca. half of the β -Mg(¹¹BD₄)₂ existed above 184 °C. Below 184 °C, the phase proportion of β -Mg(¹¹BD₄)₂ doubles. Taken together, the QPA indicates that ca. half of the crystalline β -Mg(¹¹BD₄)₂ phase forms while cooling from 350 to 200 °C, while the remaining half of crystalline β -Mg(¹¹BD₄)₂ forms below the polymorphic transition temperature, over a short temperature range from ca. 184 to 160 °C.

Our manometric analysis indicates that a total of 16.9 wt % D (stoichiometric Mg(¹¹BD₄)₂ corresponds to 25.8 wt % D) has been absorbed by the isotopic Mg¹¹B₂ sample by 400 °C. Figure 8 shows neutron diffraction data over a short 2-theta range from 38 to 45° 2θ. From this figure we can observe the large

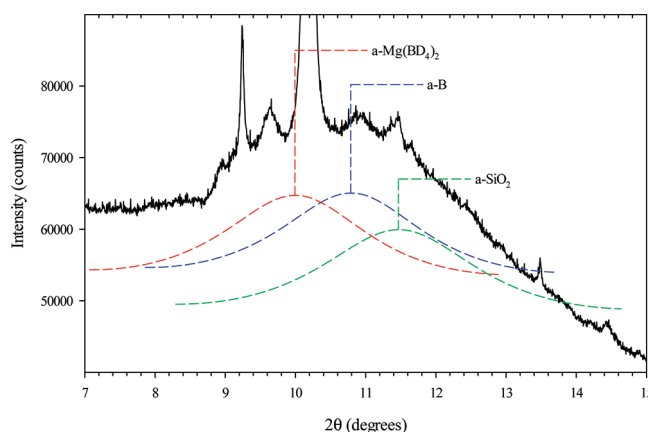


Figure 5. Zoomed image of the X-ray synchrotron data of deuterated natural $\text{MgB}_2 + 0.05\text{Al}_3\text{Ti}$, showing the three primary amorphous halos from $\text{a-Mg}(\text{BD}_4)_2$, a-B , and a-SiO_2 (quartz capillary) contributing to the broad feature running from ca. 3.80 to 5.45 Å.

reduction in the amount of crystalline Mg^{11}B_2 at 350 – 400 °C, compared to the static contribution from the stainless steel linear in the pressure cell. QPA indicates ca. two-thirds of the starting Mg^{11}B_2 is consumed to form the very broad features in Figure 6, and based on our manometry, this suggests a total composition of $\text{Mg}^{11}\text{B}_2\text{D}_{7.1}$ at 400 °C. After the absorption has stopped at 400 °C, no further absorption from the gas phase is observed during sample cooling, and a small rise in the unreacted Mg^{11}B_2 proportion is consistent with the formation of stoichiometric crystalline $\beta\text{-Mg}^{11}\text{B}_2(\text{BD}_4)_2$ during cooling. That is, the slightly substoichiometric $\text{Mg}^{11}\text{B}_2\text{D}_{7.1}$ phase(s) loses a small amount of Mg^{11}B_2 so that perfectly stoichiometric $\beta\text{-Mg}^{11}\text{B}_2(\text{BD}_4)_2$ can crystallize from it during cooling. The exact nature of the substoichiometric $\text{Mg}^{11}\text{B}_2\text{D}_{7.1}$ phase(s) at 400 °C is not clear. The fusing of the sample is highly likely to have occurred at 350 – 400 °C; however, the broad features present with a doublet. The inner core of unreacted Mg^{11}B_2 remains in a crystalline state, suggesting that the outer portion of the powder grain composed of the substoichiometric $\text{Mg}^{11}\text{B}_2\text{D}_{7.1}$ phase(s) has become molten and resolidified quickly, forming nanocrystals; otherwise, the molten state of substoichiometric $\text{Mg}^{11}\text{B}_2\text{D}_{7.1}$ would present with only a single dominant broad feature, typical of a coherently diffracting liquid phase. As such, the 10% of noncrystalline B we observe in the completely cooled sample is likely to have appeared simultaneously as the substoichiometric $\text{Mg}^{11}\text{B}_2\text{D}_{7.1}$ has become highly disordered and molten and fused the sample. It is not evident from the neutron data at 350 – 400 °C what state the 10% of B atoms is in. That the substoichiometric $\text{Mg}^{11}\text{B}_2\text{D}_{7.1}$ phase(s) appears to have quickly melted, fused the sample, and resolidified is highly reminiscent of the hydrogen absorption/desorption process for LiBH_4 . For pure LiBH_4 , hydrogen cannot enter or leave the sample below the melting point. LiBH_4 remains as an ionic liquid at least 80 °C past the melting temperature, retaining its BH_4^- units in the molten state, as evidenced by in situ Raman spectroscopy.⁵⁰ Due to the slightly substoichiometric $\text{Mg}^{11}\text{B}_2\text{D}_{7.1}$ composition at 400 °C, we infer that an ionic liquid has attempted to form which has not been able to maintain a complete charge balance and has quickly recrystallized to a nanocrystalline state, giving the two broad features at ca. 16.23 and $25.84^\circ 2\theta$ in the neutron data. If we assume that a single phase substoichiometric $\text{Mg}^{11}\text{B}_2\text{D}_{7.1}$ composition cannot exist, then $\text{Mg}^{11}\text{B}_2\text{D}_{7.1} \rightarrow 0.89\text{Mg}^{11}\text{B}_2(\text{BD}_4)_2 +$

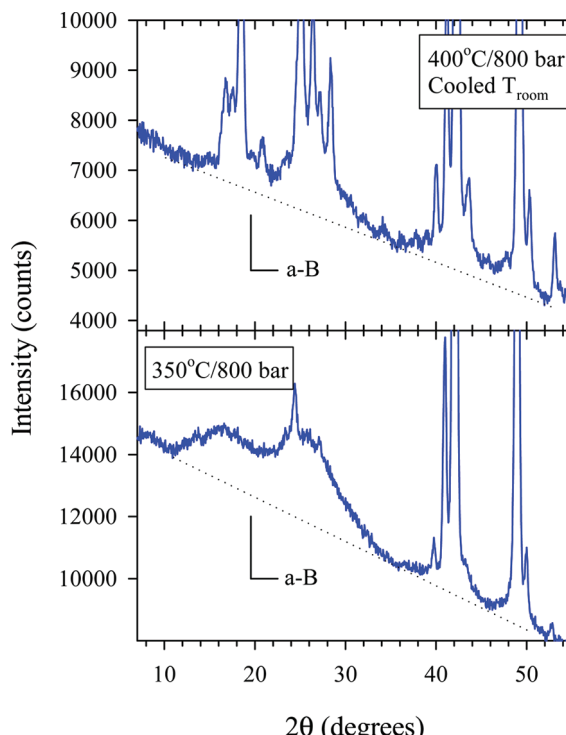


Figure 6. Background deviation observable in neutron diffraction data from deuterated isotopic $^{11}\text{MgB}_2$ around the 4.4 Å d -spacing maximum of the primary halo from amorphous B.

$0.11\text{Mg}^{11}\text{B}_2$, and we would expect unreacted Mg^{11}B_2 nanocrystals to exist within a charge balanced ionic melt. However, such unreacted Mg^{11}B_2 nanocrystals would reveal themselves by increasing the intensity of the tails of the inner core of microcrystalline Mg^{11}B_2 reflections, and we do not observe such features in our neutron data. It is to be noted, however, that MgB_2 can exist in an amorphous state,^{51,52} over a wide composition range, ca. $\text{MgB}_{1.56}$ to $\text{MgB}_{2.45}$. Thus, a completely charge balanced ionic melt can exist which ejects small nanoscopic particles of amorphous MgB_2 to maintain the charge balance. Small nanoparticles of amorphous MgB_2 would not affect the tails of the unreacted microcrystalline core of MgB_2 and would be undetectable in a minor proportion in neutron diffraction data. As such, we expect that the total substoichiometric $\text{Mg}^{11}\text{B}_2\text{D}_{7.1}$ composition at 400 °C/800 bar giving the two broad features at ca. 16.23 and $25.84^\circ 2\theta$ represents at least four solid state phases, stoichiometric nanocrystalline $\text{Mg}^{11}\text{B}_2(\text{BD}_4)_2$, unreacted amorphous Mg^{11}B_2 nanocrystals, unreacted microcrystalline Mg^{11}B_2 , and an unidentified phase(s) containing up to 10% of missing B atoms.

From the QPA analysis of the isotopic Mg^{11}B_2 sample in the cooled state after deuteration, all Mg atoms are crystallographically accounted for, and 10% of B atoms appear to be in a noncrystalline state. There is no evidence from the QPA that amorphous $\text{Mg}^{11}\text{B}_2(\text{BD}_4)_2$ exists as a minor proportion due to incomplete crystallization. This is in contrast to the natural MgB_2 sample, which in the cooled state after deuteration shows a broad feature corresponding to primary halos from both amorphous $\text{Mg}(\text{BD}_4)_2$ and amorphous B. The explanation of this difference in sample state after cooling may be found in the sample cooling rates. The isotopic sample was cooled at 0.19 °C/min, compared to 1.09 °C/min for the sample containing natural B. We expect that the significantly faster cooling of the natural B sample has

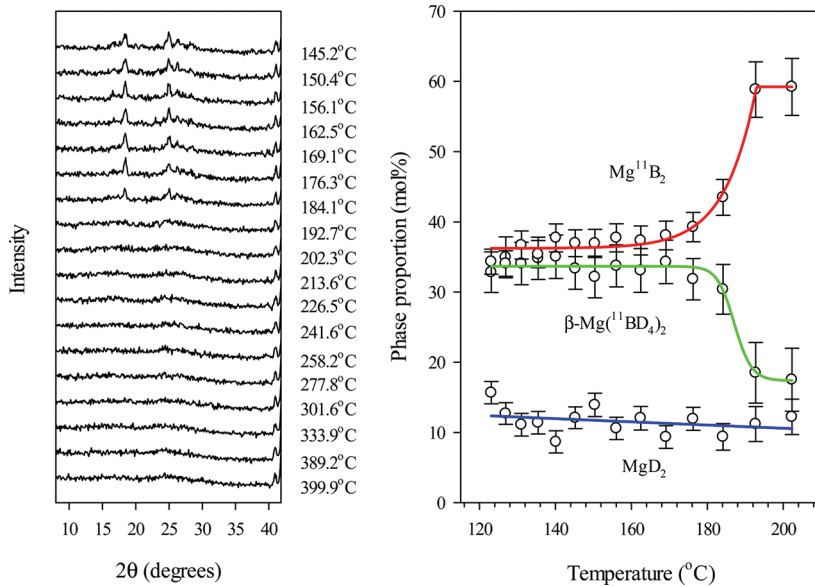


Figure 7. In situ neutron diffraction data (left figure) collected while cooling from ca. 400 to 145 °C, showing crystallization of β -Mg(¹¹BD₄)₂ (QPA in right figure) below the polymorphic transition temperature. The strongest (101) reflection from unreacted Mg¹¹B₂ can be observed at ca. 41° 2θ.

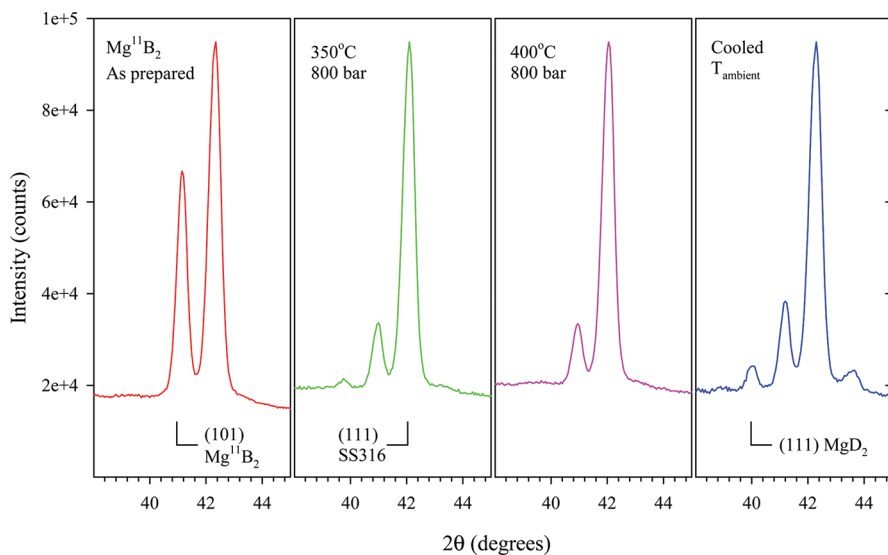


Figure 8. Amount of Mg¹¹B₂ consumed during deuteration compared to the static contribution from the SS316 linear in our pressure cell.

led to incomplete crystallization of stoichiometric crystalline Mg(BD₄)₂, leaving some of the original high temperature MgB₂D₈ “nanocrystals” in an amorphous state during cooling, realizing a minor proportion of amorphous Mg(BD₄)₂.

SEM and TEM Analysis of the Surface of Fused β -Mg(BH₄)₂. During hydrogenation/deuteration up to 400 °C and >800 bar hydrogen pressure, macroscopic-sized MgB₂ samples suffer significant fusing, particularly in a tall cylindrical geometry. Individual powder grains will fuse together in a solid glassy lump (visually black and glassy), not just at the entry point for hydrogen, but over the entire sample, indicating that the glassy phase forms at the surface of every powder grain and binds the entire sample together. After cooling, the upper portion of the fused cylindrical lump becomes rich in crystalline β -Mg(BH₄)₂ as evidenced by the formation of a white-colored powder on top

of the lump. Figure 9 shows an SEM image of a large millimeter scale piece of the fused lump that has broken away during mechanical removal of the cooled sample. The lump is highly porous on the micrometer-to-macro scale, indicating irregular fusing of powder grains has occurred under hydrogen pressure. After the total sample fusing has occurred, the entire sample will no longer absorb hydrogen, even under 350 °C and 1650 bar. The glassy phase that forms is extremely hard and requires mechanical treatment to remove specimens for study. After mechanical removal and grinding of the entire sample, the average β -Mg(BH₄)₂ yield is typically ca. 43%, with the remainder of the sample mostly unreacted microcrystalline MgB₂, bound internally within the hard black glassy phase. Such behavior would be highly problematic for kilogram-sized reversible Mg(BH₄)₂ hydrogen storage tanks, and very thin geometries would be

needed to prevent fusing. The only two reported hydrogenations of MgB₂^{22,23} both used thin pressed discs of MgB₂ but have not alluded to the problem of thicker samples fusing. Even in thin discs of MgB₂, the highest yield of β -Mg(BH₄)₂ was only 75%, indicating again that full conversion of the sample was inhibited.

Only a single TEM study of partially decomposed Mg(BH₄)₂ exists, at a point on the desorption pressure–composition isotherm (at 558 K) where MgH₂ formation has begun.³⁵ The high resolution image clearly shows MgH₂ and an amorphous phase. However, no EDS was performed, and the Mg:B ratio of the amorphous phase remains unknown. While our X-ray synchrotron data clearly show a broad feature which is consistent with the *d*-spacing of the primary amorphous halo of milled Mg(BH₄)₂,³⁰ the powder surface of milled amorphous (a-) Mg(BH₄)₂ does

not appear glassy. Our fused and cooled samples are composed of crystalline β -Mg(BH₄)₂, amorphous-Mg(BH₄)₂ formed dependent on cooling rate, unreacted MgB₂, Mg (or MgH₂), and the unknown glassy phase. Our QPA of the isotopic neutron and natural X-ray synchrotron samples indicates ca. 4–10% of B atoms are missing (all Mg is accounted for in both samples, including free unreacted Mg), implying that the hard black glassy phase is likely a B rich phase, either amorphous or highly nanocrystalline. This is further supported by the observation that crystalline β -Mg(BH₄)₂ is white in color and that amorphous-Mg(BH₄)₂ is absent in our isotopic sample, yet both the natural and isotopic samples appear black and glassy.

Figure 10 is a high resolution TEM image of the surface region of a fused lump. This region is amorphous, compared to the interior of the lump which is crystalline. The radially integrated fast Fourier transform (FFT) of the upper region in Figure 10 shows a very broad feature with a maximum immediately in the vicinity of the expected amorphous B halo at ca. 4.4 Å. Amorphous B has also been observed previously in solid state ¹¹B NMR data after the hydrogenation of MgB₂.²² No hydrogen evolution could be observed (typically evident as obvious bubbling) by knock on damage during TEM observation, suggesting no hydrogen was present in the amorphous B phase in this particular region. This is consistent with the observation that amorphous B typically contains only a moderate solid solution of hydrogen to a capacity of ca. BH_{0.25},⁵³ and we should expect regions of amorphous B that are devoid of hydrogen. Integrating the lower part of Figure 10, we also observe another broad diffraction halo at ca. 2.6 Å, which is consistent with Mg–B–O (magnesium borates) or Mg–B–O–H (hydrated magnesium borate) phases. Certain x MgO(1 – x)B₂O₃ compositions such as x = 0.8 display a primary amorphous halo at ca. 2.6 Å and also display a strong infrared absorbance at 1405–1436 cm^{−1}.⁵⁴ Hydrated magnesium borates typically display a mixture of crystalline phases but can also show a very broad feature that runs across

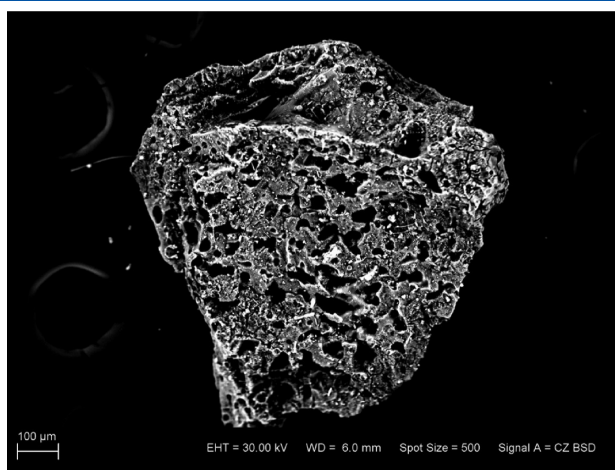


Figure 9. Backscattered electron SEM image at 30 keV of a mechanically removed large millimeter scaled fused lump formed after hydrogenation of natural MgB₂ to 400 °C and 800 bar.

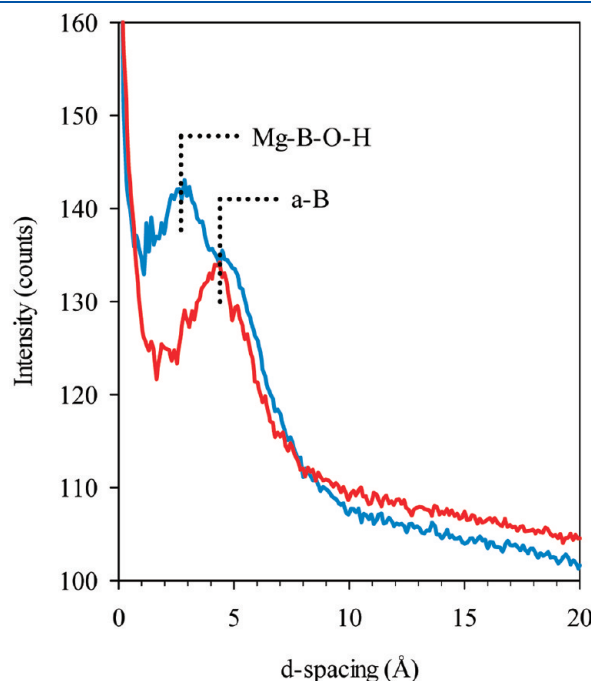
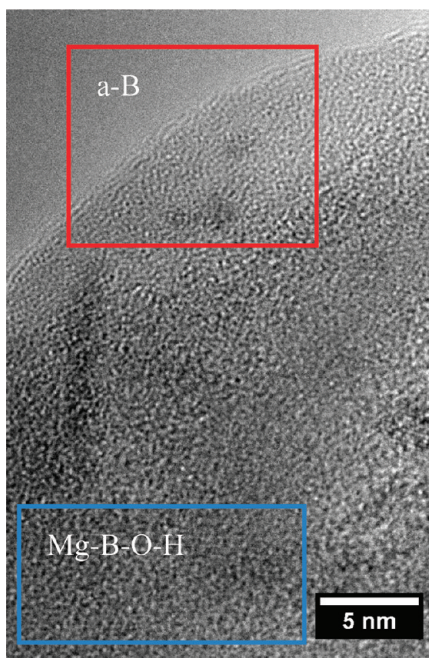


Figure 10. High resolution TEM image of the surface of the fused material (hydrided natural MgB₂ cooled to room temperature), showing an amorphous region, composed of a-B and an Mg–B–O–H phase.

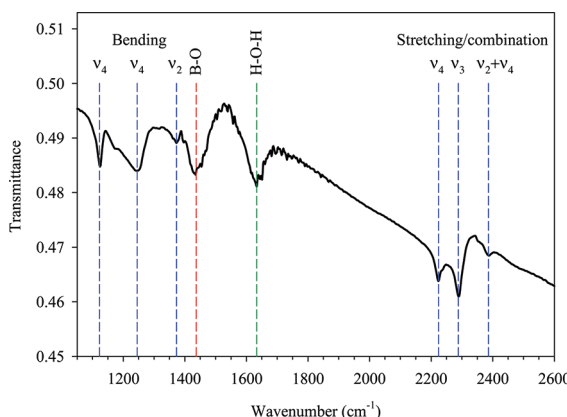


Figure 11. FT-IR spectrum of the fused MgB_2 sample after hydrogenation at $400\text{ }^\circ\text{C}$ and 800 bar. Bending and stretching modes are reported on the basis of those observed previously for $\text{Mg}(\text{BH}_4)_2$.⁵⁹

$d = 2.6\text{ \AA}$ in diffraction data.⁵⁵ Hydrated magnesium borates also display an infrared absorption band at ca. 1420 cm^{-1} .⁵⁶ In both cases, the absorbance in the 1420 cm^{-1} region is attributed to a B–O stretch; however, the hydrate also displays a band at ca. 1630 cm^{-1} from a H–O–H bending mode.⁵⁶ Both of these modes have also been observed previously in the LiBH_4 – MgH_2 system, with the B–O stretch misinterpreted as an “unknown” B–H stretch.⁵⁷ We note that while Mg–B–O–H phases can be glassy in nature, they are typically white or very light in color and cannot explain the fused black glassy phase. Further, the amorphous Mg–B–O–H phase appears morphologically behind the outer amorphous B layer. Figure 11 shows FT-IR data collected on the fused sample. We observe typical B–H stretching modes in the 2200 – 2400 cm^{-1} region which are known to be from BH_4^- units.⁵⁸ We also observe modes at 1436 and 1633 cm^{-1} , which correspond to the B–O and H–O–H modes described above. Taken together, our QPA and radially integrated FFT and FT-IR data indicate a minor component of Mg–B–O–H that is present in the surface regions of the fused sample. We also note that the starting MgB_2 (as purchased from Sigma-Aldrich and also isotopically synthesized Mg^{11}B_2) both contain significant amounts of MgO , ca. 2 – 3 mol\% . It has been noted that even at minor concentrations of MgO impurity (up to 5 mol\%), surface coverage by MgO nanocrystals on the MgB_2 surface can reach ca. 25% .⁴⁹ MgO is also evident in the first hydrogenation study.²² This MgO is highly likely to be the source of oxygen contamination which leads to the formation of an Mg–B–O–H phase which exhibits the broad halo at 2.6 \AA .

The extreme hardness of the glassy fused lump is also consistent with the known high hardness of B.⁶⁰ Single phase crystalline B is known to be highly chemically inert,⁶¹ so the formation of “near” single phase amorphous B on the outer powder surface affords an explanation of why it is difficult to conduct further hydrogen cycles. The penetration of H into solid a-B is highly likely kinetically stable, even at $400\text{ }^\circ\text{C}$. If some H can diffuse through the outer layer of a-B, the layer of Mg–B–O–H phase beneath the a-B layer is likely another kinetically stable barrier for H to break through. It is also to be noted that both the α and β $\text{Mg}(\text{BH}_4)_2$ crystal structures contain a large porous network, which could easily accommodate atomic H diffusion. This again reinforces the observation by TEM of amorphous B regions on the surface of fused lumps, which must constitute a

closed morphology, encapsulating any crystalline $\text{Mg}(\text{BH}_4)_2$ that has formed and preventing easy atomic H diffusion through the crystalline $\text{Mg}(\text{BH}_4)_2$ pores, restricting further growth of $\text{Mg}(\text{BH}_4)_2$.

CONCLUSIONS

We have obtained a ca. 43% yield of the high temperature $\beta\text{-Mg}^{(11)}\text{BD}_4)_2$ phase by direct deuteration of Mg^{11}B_2 . QPA indicates that ca. half of the crystalline $\beta\text{-Mg}^{(11)}\text{BD}_4)_2$ phase forms while cooling from 350 to $200\text{ }^\circ\text{C}$, and the remaining half of crystalline $\beta\text{-Mg}^{(11)}\text{BD}_4)_2$ forms below the polymorphic transition temperature, from ca. 184 to $160\text{ }^\circ\text{C}$. Measurements on deuterated isotopic Mg^{11}B_2 samples indicated the originally proposed structure solution⁷ needed revision based on our joint refinement of X-ray synchrotron and neutron diffraction data, to correct unphysical bond lengths and H positions. MgB_2 powder hydrided in a tall/thick cylindrical geometry suffers macroscopic sample fusing, resulting in an extremely hard fused glassy black lump, which is consistent with an amorphous phase composed predominantly of B, according to high resolution TEM and QPA of diffraction data. The formation of stoichiometric amorphous $\text{Mg}(\text{BH}_4)_2$ appears to be an artifact of the cooling process, dependent on cooling rate. It is also clear that even though diffraction data may appear “featureless” in certain stages of $\text{Mg}(\text{BH}_4)_2$ formation or decomposition, there exist strong primary halos in X-ray synchrotron data that are attributable to amorphous $\text{Mg}(\text{BH}_4)_2$ and amorphous B, at well-known d -spacing maxima. We also observe a minor proportion of Mg–B–O–H phase in the surface regions of fused samples, which corresponds to a broad diffraction halo centered at ca. 2.6 \AA . The composite layer of a-B/Mg–B–O–H on the surface of fused hydrogenated MgB_2 samples presents as a kinetically stable hydrogen impermeable layer, which will greatly restrict further hydrogen cycling.

ASSOCIATED CONTENT

S Supporting Information. Detailed information is provided regarding the crystallographic structure solution of $\beta\text{-Mg}^{(11)}\text{BD}_4)_2$. This material is available free of charge via the Internet at <http://pubs.acs.org>.

AUTHOR INFORMATION

Corresponding Author

*E-mail mark.pitt@gmail.com; tel. +61 8 9266 3673; fax +61 8 9266 2377.

ACKNOWLEDGMENT

The authors acknowledge the facilities and scientific and technical assistance of the Curtin Electron Microscopy Facility and the Australian Microscopy & Microanalysis Research Facility at the Centre for Microscopy, Characterization & Analysis, The University of Western Australia, a facility funded by The University, State and Commonwealth Governments. The authors are grateful to W. Rickard at Curtin University for his assistance with the SEM measurements. M.P.P. thanks the Queensland Synchrotron Steering Committee for the allocation of foundation investor beam time on the Powder Diffraction Beamline at the Australian Synchrotron in Melbourne. This work is based on experiments performed at the Swiss spallation neutron source SINQ, Paul Scherrer Institute, Villigen, Switzerland. Travel funds

were provided from the Access to Major Research Facilities Program, which is supported by the Commonwealth of Australia under the International Science Linkages program. M.P.P., C.E.B., and E.M.G. acknowledge the financial support of the Australian Research Council for ARC Discovery grant DP0877155. We acknowledge the facilities, scientific, and technical assistance with FTIR measurements of P. Chapman, Department of Chemistry, Curtin University of Technology, Perth, Western Australia.

■ REFERENCES

- (1) Nakamori, Y.; Miwa, K.; Ninomiya, A.; Li, H.; Ohba, N.; Towata, S.-i.; Zuttel, A.; Orimo, S.-i. *Phys. Rev. B* **2006**, *74*, 045126.
- (2) Nagamatsu, J.; Nakagawa, N.; Muranaka, T.; Zenitani, Y.; Akimitsu, J. *Nature* **2001**, *410*, 63.
- (3) Bugoslavsky, Y.; Cohen, L. F.; Perkins, G. K.; Polichetti, M.; Tate, T. J.; Gwilliam, R.; Caplin, A. D. *Nature* **2001**, *411*, 561.
- (4) Park, E. K.; Lee, J. H.; Lee, S. Y.; Moeckly, B. H.; Claassen, J. H. *Supercond. Sci. Technol.* **2008**, *21*, 075005.
- (5) Nakamori, Y.; Orimo, S.; Ekin, T.; Fujii, H. *J. Alloys Compd.* **2002**, *335*, L21.
- (6) Wiberg, E.; Bauer, R. Z. *Naturforsch. B* **1950**, *5*, 397.
- (7) Her, J.-H.; Stephens, P. W.; Gao, Y.; Soloveichik, G. L.; Rijssenbeek, J.; Andrus, M.; Zhao, J.-C. *Acta Crystallogr., Sect. B* **2007**, *63*, 561.
- (8) Černý, R.; Filinchuk, Y.; Hagemann, H.; Yvon, K. *Angew. Chem., Int. Ed.* **2007**, *46*, 5765.
- (9) Ozolins, V.; Majzoub, E. H.; Wolverton, C. *Phys. Rev. Lett.* **2008**, *100*, 135501.
- (10) Caputo, R.; Tekin, A.; Sikora, W.; Züttel, A. *Chem. Phys. Lett.* **2009**, *480*, 203.
- (11) van Setten, M. J.; Lohstroh, W.; Fichtner, M. *J. Mater. Chem.* **2009**, *19*, 7081.
- (12) Voss, J.; et al. *J. Phys.: Condens. Matter* **2009**, *21*, 012203.
- (13) Zhou, X.-F.; Qian, Q.-R.; Zhou, J.; Xu, B.; Tian, Y.; Wang, H.-T. *Phys. Rev. B* **2009**, *79*, 212102.
- (14) Filinchuk, Y.; Černý, R.; Hagemann, H. *Chem. Mater.* **2009**, *21*, 925.
- (15) Dai, B.; Sholl, D. S.; Johnson, J. K. *J. Phys. Chem. C* **2008**, *112*, 4391.
- (16) van Setten, M. J.; de Wijs, G. A.; Fichtner, M.; Brocks, G. *Chem. Mater.* **2008**, *20*, 4952.
- (17) Lstrokodziana, Z.; van Setten, M. J. *Phys. Rev. B* **2010**, *81*, 024117.
- (18) Soloveichik, G. L.; Andrus, M.; Gao, Y.; Zhao, J. C.; Kniajanski, S. *Int. J. Hydrogen Energy* **2009**, *34*, 2144.
- (19) George, L.; Drozd, V.; Saxena, S. K.; Bardaji, E. G.; Fichtner, M. *J. Phys. Chem. C* **2008**, *113*, 486.
- (20) Konoplev, V. N.; Bakulina, V. M. *Russ. Chem. Bull.* **1971**, *20*, 136.
- (21) Yang, J.; Zhang, X.; Zheng, J.; Song, P.; Li, X. *Scr. Mater.* **2011**, *64*, 225.
- (22) Severa, G.; Ronnebro, E.; Jensen, C. M. *Chem. Commun.* **2010**, *46*, 421.
- (23) Newhouse, R. J.; Stavila, V.; Hwang, S.-J.; Klebanoff, L. E.; Zhang, J. *Z. J. Phys. Chem. C* **2010**, *114*, 5224.
- (24) Zaleski, A. J.; Iwasieczko, W.; Kaczorowski, D.; Drulis, H.; Tkacz, M.; Zogal, O. J.; Klamut, J. *Low Temp. Phys.* **2001**, *27*, 780.
- (25) Du, A. J.; Smith, S. C.; Yao, X. D.; Sun, C. H.; Li, L.; Lu, G. Q. *J. Nanosci. Nanotechnol.* **2009**, *9*, 4388.
- (26) Wiberg, V. E.; Bauer, R. Z. *Naturforsch. B* **1952**, *7*, 58.
- (27) Stasinevich, D. S.; Egorenko, G. A. *Zh. Neorg. Khim.* **1968**, *13*, 654.
- (28) Soulié, J. P.; Renaudin, G.; Černý, R.; Yvon, K. *J. Alloys Compd.* **2002**, *346*, 200.
- (29) Filinchuk, Y.; Ronnebro, E.; Chandra, D. *Acta Mater.* **2009**, *57*, 732.
- (30) Li, H. W.; Kikuchi, K.; Nakamori, Y.; Miwa, K.; Towata, S.; Orimo, S. *Scr. Mater.* **2007**, *57*, 679.
- (31) Chlopek, K.; Frommen, C.; Leon, A.; Zabara, O.; Fichtner, M. *J. Mater. Chem.* **2007**, *17*, 3496.
- (32) Hanada, N.; Chlopek, K.; Frommen, C.; Lohstroh, W.; Fichtner, M. *J. Mater. Chem.* **2008**, *18*, 2611.
- (33) Li, H. W.; Kikuchi, K.; Nakamori, Y.; Ohba, N.; Miwa, K.; Towata, S.; Orimo, S. *Acta Mater.* **2008**, *56*, 1342.
- (34) Matsunaga, T.; Buchter, F.; Miwa, K.; Towata, S.; Orimo, S.; Züttel, A. *Renew. Energy* **2008**, *33*, 193.
- (35) Li, H. W.; et al. *Nanotechnology* **2009**, *20*, 204013.
- (36) Pistidda, C.; Garroni, S.; Dolci, F.; Bardaji, E. G.; Khandelwal, A.; Nolis, P.; Dornheim, M.; Gosalawit, R.; Jensen, T.; Cerenius, Y.; Suriñach, S.; Baró, M. D.; Lohstroh, W.; Fichtner, M. *J. Alloys Compd.* **2010**, *508*, 212.
- (37) Soloveichik, G. L.; Gao, Y.; Rijssenbeek, J.; Andrus, M.; Kniajanski, S.; Bowman, R. C., Jr; Hwang, S.-J.; Zhao, J.-C. *Int. J. Hydrogen Energy* **2009**, *34*, 916.
- (38) Hwang, S.-J.; Bowman, R. C.; Reiter, J. W.; Rijssenbeek; Soloveichik, G. L.; Zhao, J.-C.; Kabour, H.; Ahn, C. C. *J. Phys. Chem. C* **2008**, *112*, 3164.
- (39) Chong, M.; Karkamkar, A.; Autrey, T.; Orimo, S.-i.; Jalilatgi, S.; Jensen, C. M. *Chem. Commun.* **2011**, *47*, 1330.
- (40) Ozolins, V.; Majzoub, E. H.; Wolverton, C. *J. Am. Chem. Soc.* **2009**, *131*, 230.
- (41) Zhang, Y.; Majzoub, E.; Ozolincedilcaron, V.; Wolverton, C. *Phys. Rev. B* **2010**, *82*, 174107.
- (42) Chen, X.; Lingam, H. K.; Huang, Z.; Yisgedu, T.; Zhao, J.-C.; Shore, S. G. *J. Phys. Chem. Lett.* **2009**, *1*, 201.
- (43) Hinks, D. G.; Jorgensen, J. D.; Zheng, H.; Short, S. *Physica C: Superconductivity* **2002**, *382*, 166.
- (44) Gray, E. M.; Bailey, I. F. *J. Neutron Res.* **2008**, *16*, 127.
- (45) Hunter, B. A. *Commission Powder Diffraction Newsletter* **1998**, *20*, 21.
- (46) Vullum, P. E.; Pitt, M. P.; Walmsley, J. C.; Hauback, B. C.; Holmestad, R. *J. Alloys Compd.* **2011**, *509*, 281.
- (47) Filinchuk, Y.; Richter, B.; Jensen, T. R.; Dmitriev, V.; Chernyshov, D.; Hagemann, H. *Angew. Chem., Int. Ed.* **2011**, DOI: DOI: 10.1002/anie.201100675.
- (48) Gillespie, J. S. *J. Am. Chem. Soc.* **1966**, *88*, 2423.
- (49) Jiang, J.; et al. *Supercond. Sci. Technol.* **2006**, *19*, L33.
- (50) Reed, D.; Book, D. *Mater. Res. Soc. Symp. Proc.* **2010**, *1216*, 172.
- (51) Okuma, S.; Togo, S.; Amemori, K. *Phys. Rev. B* **2003**, *67*, 172508.
- (52) Gao, Y. D.; Ding, J.; Rao, G. V. S.; Chowdari, B. V. R.; Sun, W. X.; Shen, Z. X. *Phys. Status Solidi A* **2002**, *191*, 548.
- (53) Wang, P.; Orimo, S.; Tanabe, K.; Fujii, H. *J. Alloys Compd.* **2003**, *350*, 218.
- (54) Karakassides, M. A.; Petridis, D.; Mousdis, G.; Trapalis, C.; Kordas, G. *J. Non-Cryst. Solids* **1996**, *202*, 198.
- (55) Dou, L.; Zhong, J.; Wang, H. *Phys. Scr.* **2010**, *T139*, 014010.
- (56) Yongzhong, J.; Shiyang, G.; Shuping, X.; Jun, L. *Spectrochim. Acta, Part A* **2000**, *56*, 1291.
- (57) Bösenberg, U.; Ravnsbæk, D. B.; Hagemann, H.; D'Anna, V.; Minella, C. B.; Pistidda, C.; van Beek, W.; Jensen, T. R.; Bormann, R. d.; Dornheim, M. *J. Phys. Chem. C* **2010**, *114*, 15212.
- (58) Hagemann, H.; D'Anna, V.; Rapin, J.-P.; Yvon, K. *J. Phys. Chem. C* **2010**, *114*, 10045.
- (59) Giannasi, A.; Colognesi, D.; Ulivi, L.; Zoppi, M.; Ramirez-Cuesta, A. J.; Bardaji, E. G.; Roehm, E.; Fichtner, M. *J. Phys. Chem. A* **2010**, *114*, 2788.
- (60) Solozhenko, V.; Kurakevych, O.; Organov, A. *J. Superhard Mater.* **2008**, *30*, 428.
- (61) Corey, E. *J. Chem. Eng. News* **2003**, *81*, 40.